JGR Atmospheres

RESEARCH ARTICLE
10.1029/2021JD035273

Long-Term Variation and Source Apportionment of Black Carbon at Mt. Waliguan, China

Mingming Dai[1], Bin Zhu[1], Chenwei Fang[1], Shunwu Zhou[1], Wen Lu[1], Delong Zhao[2], Deping Ding[2], Chen Pan[3], and Hong Liao[1]

[1]Collaborative Innovation Centre on Forecast and Evaluation of Meteorological Disasters, Key Laboratory of Meteorological Disaster, Ministry of Education (KLME), Joint International Research Laboratory of Climate and Environment Change (ILCEC), Nanjing University of Information Science & Technology, Nanjing, China, [2]Beijing Weather Modification Office, Beijing, China, [3]Jiangsu Meteorological Observatory, Nanjing, China

Abstract Black carbon (BC) is a significant driver of global climate change, and its long-term variation is affected by a combination of anthropogenic activities and meteorological diffusion conditions. However, distinguishing the effects of these two factors on BC variation has proven difficult. In this study, we used the China Black Carbon Observational Network data set to assess the diurnal, seasonal, and long-term BC trends at Mt. Waliguan (WLG) from 2008 to 2017. The mean BC concentration at WLG was 449 ± 366 ng/m^3, with a decreasing trend of 2 %yr^{-1}, which was mainly related to emission reduction measures in China. The BC concentration at WLG was higher under easterly air masses than that under westerly air masses, which suggests that the former are conducive to BC transport from the highly polluted eastern regions. Due to the origin and velocity of air masses, the BC concentration at WLG in summer is higher than that in winter. The intensity of the Tibetan Plateau monsoon had an important positive influence on the easterly air masses frequency, which modulated BC transport to WLG in summer. According to the concentration-weighted trajectory analysis, the high-potential BC source regions were distributed in Lanzhou, Chengdu, and Xi'an urban agglomerations as well as in northern India. Community Atmosphere Model 5 simulations with a BC-tagging technique inferred North Central China, Northwest China, and Indian Peninsula to be the major BC source regions to WLG, accounting for 56.1%, 17.5%, and 12.1% of the total BC, respectively.

Plain Language Summary In this study, we investigated the long-term variation of black carbon (BC) between 2008 and 2017 at Mt. Waliguan (WLG) in northeast of Tibetan Plateau, the only atmospheric baseline station in the Eurasian hinterland. A decreasing trend of BC was observed at WLG, which can be attributed to emission reduction measures in China during this period. We also found that easterly air masses promoted the transport of BC to the Tibetan Plateau from highly polluted eastern urban agglomerations of China, especially in summer. Moreover, the interannual variation of Tibetan Plateau monsoon affects the easterly air mass frequency and modulates the concentration and sources of BC at WLG. Furthermore, we identified the dominant source regions of BC to WLG.

Key Points:

- The decreasing trend and distinct seasonal variation of black carbon (BC) are mainly related to emission reduction and air mass change, respectively
- The Tibetan Plateau monsoon affects the interannual easterly air mass frequency and modulates BC sources at Mt. Waliguan (WLG) in summer
- The main BC source regions of WLG are located in North Central China, Northwest China, and Indian Peninsula

Supporting Information:

Supporting Information may be found in the online version of this article.

Correspondence to:

B. Zhu,
binzhu@nuist.edu.cn

Citation:

Dai, M., Zhu, B., Fang, C., Zhou, S., Lu, W., Zhao, D., et al. (2021). Long-term variation and source apportionment of black carbon at Mt. Waliguan, China. *Journal of Geophysical Research: Atmospheres*, *126*, e2021JD035273. https://doi.org/10.1029/2021JD035273

Received 16 MAY 2021
Accepted 9 OCT 2021

Author Contributions:

Conceptualization: Bin Zhu
Data curation: Delong Zhao, Deping Ding
Formal analysis: Wen Lu
Investigation: Delong Zhao
Methodology: Mingming Dai, Bin Zhu, Chenwei Fang, Shunwu Zhou, Chen Pan
Project Administration: Bin Zhu
Software: Mingming Dai, Chenwei Fang
Supervision: Bin Zhu, Wen Lu, Hong Liao
Validation: Chen Pan
Visualization: Mingming Dai
Writing – original draft: Mingming Dai
Writing – review & editing: Mingming Dai

1. Introduction

Black carbon (BC) is an important component of atmospheric aerosols and is mainly formed by the incomplete combustion of biomass and fossil fuels (Q. Wang, Schwarz, et al., 2014; X. Wang, Xu, & Ming, 2014). Much focus has been placed on BC over the past 20 years due to its significant impacts on air quality, climate change, and human health (Deng et al., 2008; Koelmans et al., 2006; Zhou et al., 2012). Studies have shown that the risks of exposure to high levels of BC were closely associated with cardiovascular mortality and morbidity (Janssen et al., 2011; Lin et al., 2019; Pani et al., 2020). BC strongly absorbs solar radiation, which affects the vertical temperature structure of the atmosphere (Babu et al., 2002). The deposition of BC on snow and sea ice can also accelerate their melting rate. Due to its relatively strong positive climate forcing effect, BC is considered a major contributor to global warming after carbon dioxide (CO_2) and methane (CH_4) on a global scale (Bond et al., 2013; Hansen & Nazarenko, 2004; Menon et al., 2002).

Owing to its dense population and rapid economic development, China is the main contributor of global BC concentration (Bond et al., 2013; B. Li et al., 2016). High levels of BC concentrations are mainly distributed

in megacities of the Yangtze River Delta (YRD) and North China Plain (NCP) with large population and developed industry (Ji et al., 2017; Joshi et al., 2021; Peng et al., 2019). Regional transport and biomass combustion are also important contributors (Lu et al., 2019; Zhuang et al., 2014). Affected by different weather patterns and precipitation, the lifetime of BC is approximately 4–12 days (Cape et al., 2012). Moreover, its average transport distance is >1,000 km from its source (Byčenkienė et al., 2011; Cerqueira et al., 2010; Rodhe et al., 1972). The BC concentration at a site changes with the origins of the air masses and the conditions of atmospheric diffusion. M. Wang et al. (2016) used backward trajectory analysis to study air pollutants at Ranwu (southeastern Tibetan Plateau [TP]) and found that high BC air masses were mainly sourced from southern Asia. Chen et al. (2018) found that in the nonmonsoon season, the high BC air masses at Mt. Everest (central Himalayas) mainly come from Pakistan, northern India, and Nepal due to biomass burning. During the monsoon season, the air masses from the Arabian Sea and the Bay of Bengal are relatively clean.

The BC in Darjeeling in the eastern Himalayas is mainly sourced from the Indo-Gangetic Plain and Nepal (Sarkar et al., 2019). Based on a previous analysis in the Muztagh Ata Mountain in the western TP, an air mass from inland China was found to have relatively high BC concentrations (Cao et al., 2009). Using the Community Atmosphere Model version 5 (CAM5) with source-tagging techniques, R. Zhang et al. (2015) found that biomass and fossil fuel burning in South Asia were the highest BC contributors to the Himalayas and central TP, while East Asia was the dominant source of BC to the northeast TP (all year) and southeast TP (in summer). The TP and surrounding areas are typically affected by midlatitude westerlies in winter and the Asian monsoon in summer (Wu et al., 2012). Most previous studies on BC over the TP have focused on the origin of polluted air masses, but few have explored the causes for air mass change (Cao et al., 2009; Chen et al., 2018; Q. Wang, Schwarz, et al., 2014; X. Wang, Xu, & Ming, 2014). Due to its unique geographical location and altitude, the TP has a significant influence on the atmospheric circulation of East Asia and affects the regional transport of pollutants. Mt. Waliguan (WLG) is located on the northeast slope of the TP and is the only global atmospheric baseline station in the Eurasian hinterland.

Long-term monitoring of BC in remote areas is important for assessing regional BC budgets as well as the global BC cycle. In this study, we analyzed the characteristics and long-term variation of BC at WLG by using the data set from the China Black Carbon Observational Network (CBNET) from 2008 to 2017; furthermore, the influence of different air masses on seasonal BC variation was analyzed. The contributions from potential BC source regions were identified through concentration-weight trajectory analysis and quantified by CAM5 with the BC-tagging technique. In addition, we analyzed the Tibetan Plateau monsoon index to explore its influence on the easterly air mass frequency and the regional transport of BC to WLG.

2. Data and Methods

2.1. Site Description

This study used the ground observation data of BC concentration at WLG from January 2008 to December 2017 (data set from CBNET). The CBNET is established by the China Meteorological Administration (CMA) and comprises a total of 68 stations that have been collecting data since 2006. In this study, stations with data lengths greater than 6 years were selected to ensure statistical significance. The location and spatial distribution of average BC concentrations at selected stations are shown in Figure 1, and details of the study stations can be found in Y. Zhang, Li, et al. (2019). WLG (100.89°E, 36.28°N) has an altitude of 3,816 m and is surrounded by arid/semiarid land and scattered grasslands. As the Global Atmospheric Watch (GAW) Baseline Station, WLG is located away from industrial point sources and populated regions and is therefore less directly affected by local anthropogenic activities.

2.2. Observation Instruments and Data

Long-term observations of surface BC at WLG were conducted by using AE31 (Magee Scientific, USA), which provided continuous measurements of BC concentration by measuring the optical attenuation through a quartz filter tape on which the ambient particles are forced to impinge. The aethalometer can measure the optical transmission of carbon-containing aerosols at seven wavelengths (370, 470, 520, 590, 660, 880, and 950 nm) that in turn identifies the source and size of aerosols. The BC mass concentration was calculated based on the change in optical attenuation at 880 nm because BC particles have strong

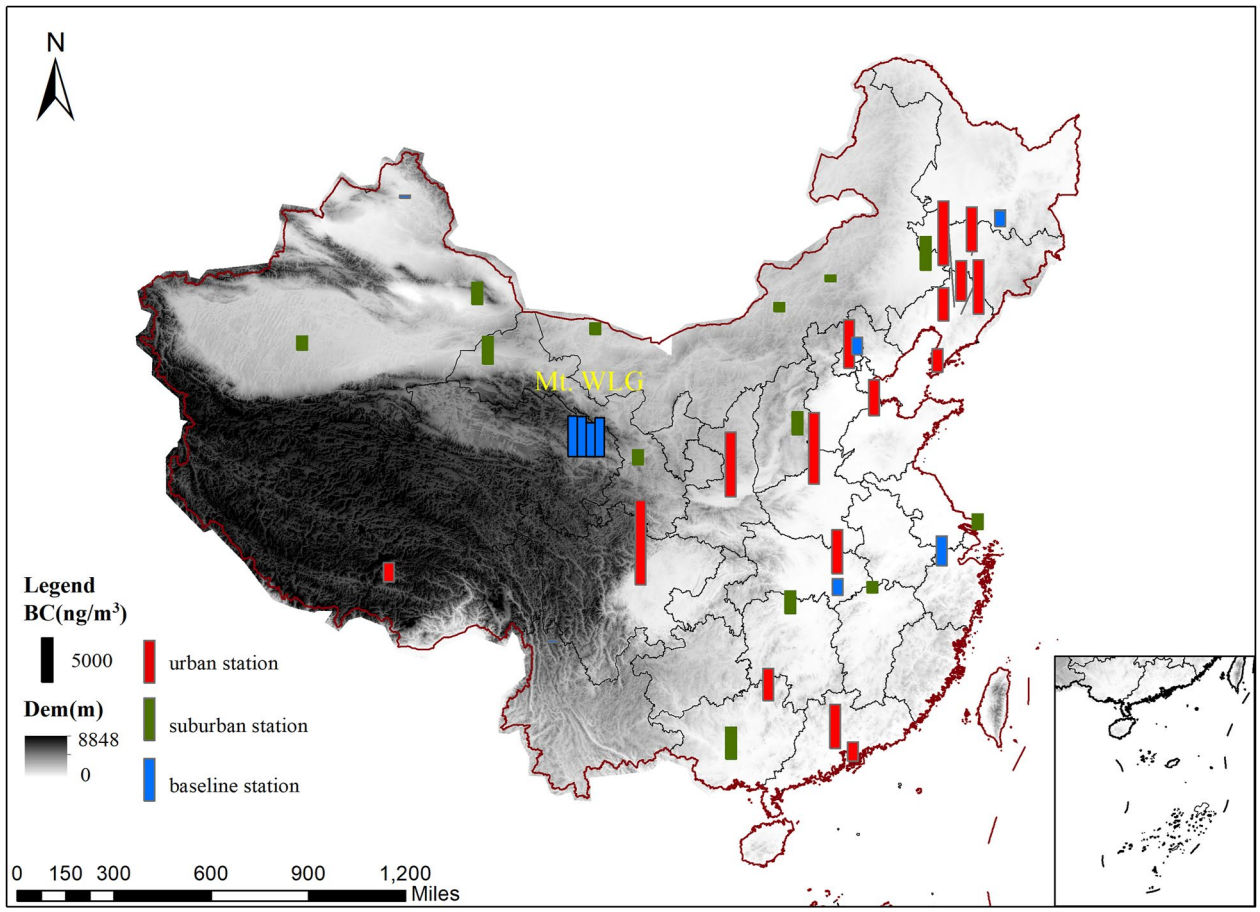

Figure 1. Spatial distribution of annual mean black carbon (BC) concentration (histograms) at 36 stations of China Black Carbon Observational Network. Among them, red indicates urban station, green indicates suburban station, and blue indicates baseline station. (Average BC concentration at Waliguan is shown in spring, summer, autumn, and winter and the values are multiplied by 10 in Figure 1).

absorption in this channel. The sampling flow was 2–5 L/min, and the data were acquired every 5 min. A zero check was done regularly to ensure that the aethalometer ran stably and smoothly.

Considering factors such as instrument maintenance and malfunctions, the quality control of the BC data was conducted prior to the research. When the sample data are less than 0, we would delete it as an abnormal value. To make the data representative, it was considered invalid if the number of samples was <60% of the total number when calculating the hourly/monthly BC concentration. As the measurements were carried out in a baseline station, where the BC concentration is expected to be very low, so we used 3σ rule method to remove the outliers. Finally, a total of 73,530 average hourly measurements were selected for further analyses, accounting for 83.9% of the total data. The proportion of valid data in each month is shown in Figure S1.

2.3. Concentration-Weighted Trajectory

The concentration-weighted trajectory (CWT) method was established by Seibert et al. (1994). In this study, the area of concern was divided into 0.5° × 0.5° grids. When the associated trajectory passed through the grid cell (i, j), each grid point was given a weighted value obtained by averaging the sample data observed at the receiver location. The calculation formula was as follows:

$$C_{ij} = \frac{\sum_{k=1}^{v} C_k \tau_{ijk}}{\sum_{k=1}^{v} \tau_{ijk}} \cdot W\left(n_{ij}\right) \quad (1)$$

$$W\left(n_{ij}\right) = \begin{cases} 1.0 & 3n_{ave} < n_{ij} \\ 0.7 & 1.5n_{ave} < n_{ij} \le 3n_{ij} \\ 0.4 & n_{ave} < n_{ij} \le 1.5n_{ave} \\ 0.17 & n_{ij} \le n_{ave} \end{cases} \quad (2)$$

where C_{ij} is the weighted average concentration in grid cell (i, j), C_k is the measured BC concentration corresponding to the trajectory passing through the grid cell (i, j), τ_{ijk} is the residence time of backward trajectory in the grid cell (i, j), $W(n_{ij})$ is the weight function, n_{ave} is the average number of trajectory points in all meshes for at least one trajectory point, and n_{ij} is the number of trajectory points in the grid cell (i, j). A high C_{ij} value indicates that the grid cell greatly contributes to BC concentration at WLG.

The data required for CWT accessed from the NCEP Global Data Assimilation System database (gdas1).

2.4. Dynamically Normalized Seasonality Monsoon Index (MI)

The dynamical normalized seasonality MI is defined as follows:

$$\delta = \frac{\left\| \overline{V_1} - V_i \right\|}{\left\| \bar{V} \right\|} - 2 \quad (3)$$

where $\overline{V_1}$ and V_i are the January climatological and monthly wind vectors, respectively, at a given point, and $\bar{V}$ is the mean of January and July climatological wind vectors at the same point. The norm $\|A\|$ is defined as $\|A\| = \left(\iint_S |A|^2 \, dS \right)^{1/2}$, where S denotes the domain of integration.

$$\| A_{i,j} \| \approx \sqrt{\alpha} \left(\left(\left| A_{i-1,j}^2 \right| + \left| A_{i,j}^2 \right| + \left| A_{i+1,j}^2 \right| \right) \cos \varphi_j + \left| A_{i,j-1}^2 \right| \cos \varphi_{j-1} + \left| A_{i,j+1}^2 \right| \cos \varphi_{j+1} \right) \quad (4)$$

where α is the mean radius of the earth and φ_j is the latitude at point (i, j). More detailed descriptions and applications of the dynamical normalized seasonality MI are presented by J. P. Li and Zeng (2002, 2003).

3. Results and Discussion

3.1. Regional Features, Trends, and Diurnal Variations of BC

As shown in Figure 1, the BC concentration in urban stations (2,228–9,691 ng/m^3) in China was much higher than that in suburban stations (733–4,006 ng/m^3) and the baseline station (300–3,615 ng/m^3). High BC values were mainly located in urban stations in eastern and central China, which are consistent with the findings by X. Y. Zhang et al. (2008). The BC concentration showed large spatial differences, with higher levels in the eastern sites of WLG compared to the western sites, which is in accordance with the regional pollutant concentration distribution in China (R. Li et al., 2019). Different from the characteristics of BC concentration higher in winter than in summer in most parts of China (Y. Zhang, Li, et al., 2019), the seasonal average BC concentration at WLG ranks from high to low as follows: spring (486 ng/m^3) ≈ summer (484 ng/m^3) > winter (465 ng/m^3) > autumn (406 ng/m^3). As a baseline station, air pollution at WLG is less directly affected by local anthropogenic activities and is mainly affected by regional transport (Fu et al., 2012; Zhu et al., 2016).

In this study, a $KZ_{(365,3)}$ filter (Kolmogorov-Zurbenko filter, 365-day length with three iterations), which can remove cycles of <632 days (1.7 years), was used to extract the long-term BC trend (Kang et al., 2019) from BC data. As shown in Figure 2a, the BC concentration at WLG showed a decreasing trend over the past 10 years, especially from 2009 to 2014. The daily BC concentration varied from 11 to 2225 ng/m^3, and the

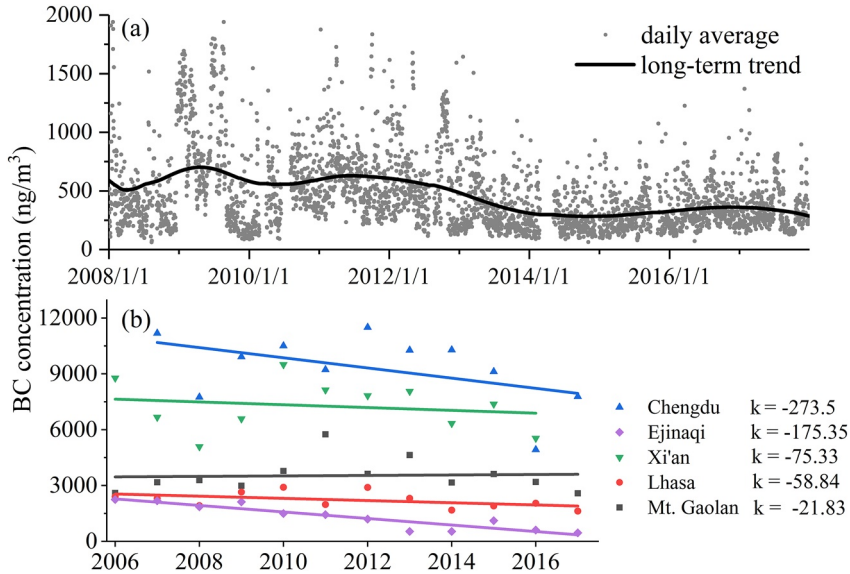

Figure 2. Time series of black carbon (BC) concentration at Waliguan (WLG) (the daily mean in dots and long-term trend in line) from 2008 to 2017 (a). Annual average BC concentration at stations (Lhasa, 91.11°E, 29.64°N; Chengdu, 104.06°E, 30.57°N; Xi'an, 108.96°E, 34.48°N; Ejinaqi, 101.06°E, 41.95°N; and Mt. Gaolan, 103.84°E, 36.02°N) around WLG (b).

annual mean concentration was 449 ng/m^3 with a standard deviation of 366 ng/m^3. As shown in Table 1, the Mann-Kendall test (Kendall, 1975) and Daniel test (Q. Zhang, Yu, et al., 2019) are statistically significant ($P < 0.05$) in winter and spring and show a significant decreasing trend of BC, and it can be seen from Theil-Sen slope (Sarkar et al., 2019) that the magnitude of the change is also large. In contrast, the decreasing trend in summer and autumn is not as obvious as that in winter and spring. For the annual average, the Mann-Kendall test shows a decreasing trend representing a nonsignificant condition but Daniel test confirmed this trend.

The diurnal BC concentration at WLG peaked at noon and was mainly affected by transport and diffusion conditions. In contrast, the diurnal BC concentration in urban areas mainly reflects the diurnal BC emission characteristics and diffusion conditions. Specifically, the BC concentration showed bimodal diurnal variation in response to traffic emissions and diffusion conditions during the rush hours (Rajesh & Ramachandran, 2017; Trompetter et al., 2013). However, the mountain site is less directly affected by local anthropogenic activities and its diurnal variation of BC concentration is mainly related to the atmospheric transport and diffusion conditions. Figure 3 illustrates the diurnal variations of the BC concentration at WLG and other two mountain sites (Mt. Lu, 1,165 m; Mt. Gaolan, 2,075 m) in the same period. The BC concentration is higher in daytime than at night, and the peak appears at noon may be due to the development of the planetary boundary layer (PBL) and pollution lifting with the valley breeze during the day (Pan et al., 2011).

Table 1
Trends of BC Concentration at WLG

	Mann-Kendall test	Daniel test	Theil-Sen slope
Year	−1.61	−0.67[a]	−44.6[a]
Spring	−1.97[a]	−0.68[a]	−45.5[a]
Summer	−0.89	−0.37	−26.2
Autumn	−0.72	−0.39	−3.9
Winter	−2.50[a]	−0.82[a]	−47.8[a]

Note. BC, black carbon; WLG, Waliguan.
[a]Pass the 0.05 significance test.

3.2. Factors Affecting Seasonal and Long-Term Variations of BC

As described in Section 3.1, we observed distinct seasonal BC variation (summer > winter) at WLG, which was notably different from that in eastern China stations. To further understand the seasonal variation and decreasing trend of BC concentration, the possible causes are discussed according to the velocity and the origin of air masses at WLG.

This research uses the Hybrid Single-Particle Lagrangian Integrated Trajectory (HYSPLIT) model with National Centers for Environmental Prediction/National Center for Atmospheric Research (NCEP/NCAR) global reanalysis meteorological data and calculates the backward trajectories starting from WLG. The incoming direction and velocity of air masses at

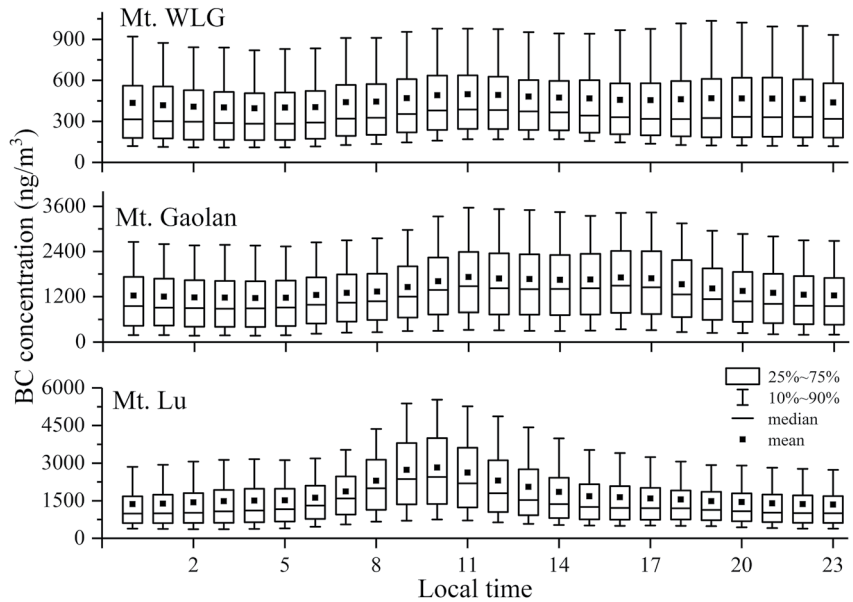

Figure 3. Diurnal variation of black carbon concentration at Mt. Waliguan (100.89°E, 36.28°N, 3,816 m), Mt. Gaolan (103.84°E, 36.02°N, 1,165 m), and Mt. Lu (115.97°E, 29.54°N, 2,075 m). The solid squares are mean values. The top and bottom short lines indicate 10% and 90% quantiles, respectively. The rectangle represents the 25% and 75% quantiles, and the inner short line of the rectangle is the median.

WLG are calculated by studying the trajectory data. Based on the analysis of 12-hr backward trajectories, we found the average zonal velocity of the air masses is 12 times the meridional velocity, and air masses from east and west direction account for 88.3% of the total data. It can be seen from Figure 1 that there is a significant difference in BC concentration between the eastern and western WLG stations. Therefore, this study compared the difference between the easterly and westerly air masses.

3.2.1. Influence of Easterly and Westerly Air Masses on Seasonal BC Variation

From 2008 to 2017, the average BC concentration under the easterly and westerly air masses at WLG was 498 and 381 ng/m^3, respectively. Air masses from east direction could carry relatively high BC to WLG. The eastern parts of WLG have a higher population density and more developed industries, resulting in a more serious air pollution. In contrast, the western parts are sparsely populated with less severe air pollution. As a result, the seasonal BC concentration variation under westerly air masses at WLG is relatively small, with a BC concentration range of 355–501 ng/m^3. In contrast, the seasonal BC concentration under easterly air masses showed notable seasonal variation of 446–897 ng/m^3 (Figure 4). We observed positive differences in the seasonal average BC concentration at WLG between the easterly and westerly air masses, with maximum differences in winter (421 ng/m^3) and minimum differences in summer (68 ng/m^3). The easterly air mass frequency at WLG varied significantly throughout the year, increasing from January to July and decreasing from August to December. The velocity of the westerly air masses showed a large seasonal variation, with the highest in winter and lowest in summer, while the seasonal variation of easterly air masses was small.

The seasonal BC variation at WLG was closely related to velocity, frequency, and BC concentration of different origin air masses. To clearly distinguish their contributions to the BC variation, the BC concentration at WLG was expressed as follows:

$$\mathrm{BC}_i = \frac{\sum_{j=1}^{m}\mathrm{BC}e_{\mathrm{ij}} + \sum_{j=1}^{n}\mathrm{BC}w_{\mathrm{ij}}}{m+n} \tag{5}$$

where i is the month, BC_i is the average BC concentration in month i, $\mathrm{BC}e_{\mathrm{ij}}$ and $\mathrm{BC}w_{\mathrm{ij}}$ represent the mean hourly BC concentration at time j in month i under the easterly and westerly air masses, m and n represent

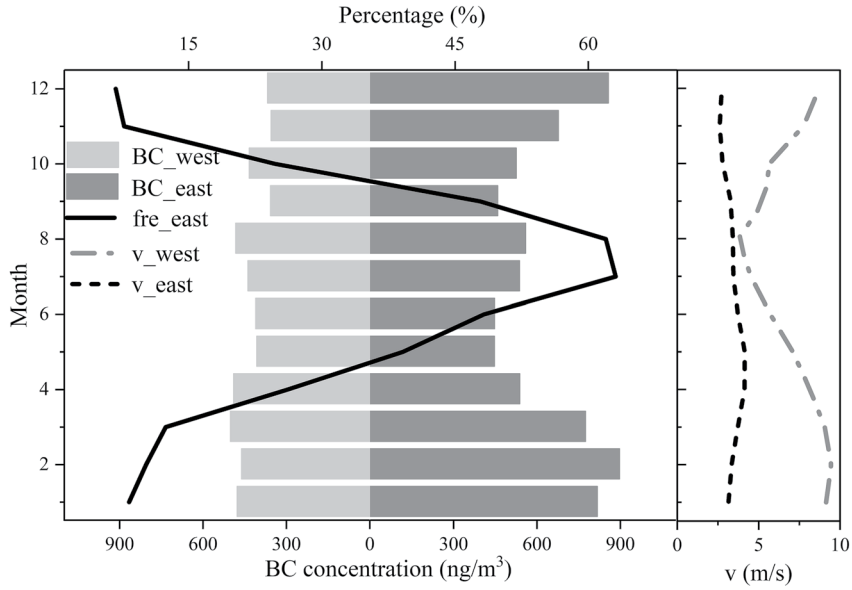

Figure 4. Monthly black carbon (BC) concentration, velocity, and frequency of different origin air masses at Waliguan. The dark/light gray histogram shows the monthly average BC concentration under the easterly/westerly air masses (ng/m^3), the black solid line shows monthly easterly air mass frequency (%), and black and gray dashed lines show the monthly velocity of the easterly and westerly air masses, respectively (m/s).

the total frequency of easterly and westerly air masses in month *i*. For month *i*, the easterly air mass frequency and the average BC concentrations under the easterly/westerly air masses at WLG can be expressed as follows:

$$\tau_i = \frac{m}{m+n} \tag{6}$$

$$\mathrm{BC}e_i = \frac{1}{m}\sum_{j=1}^{m}\mathrm{BC}e_{\mathrm{ij}} \tag{7}$$

$$\mathrm{BC}w_i = \frac{1}{n}\sum_{j=1}^{n}\mathrm{BC}w_{\mathrm{ij}} \tag{8}$$

where τ_i is the easterly air mass frequency in month *i*, $\mathrm{BC}e_i$ and $\mathrm{BC}w_i$ represent the average BC concentration under the easterly and westerly air masses in month *i*. Therefore, Equation 5 can be expressed as follows:

$$\mathrm{BC}_i = \mathrm{BC}e_i \times \tau_i + \mathrm{BC}w_i \times \left(1-\tau_i\right) \tag{9}$$

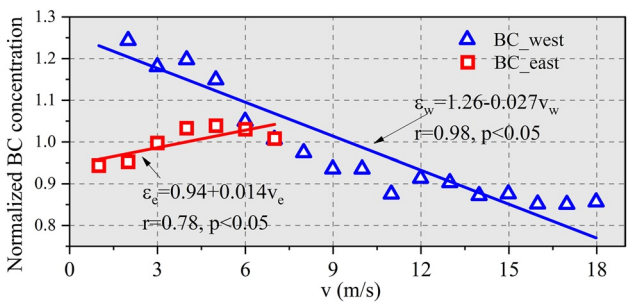

Figure 5. Normalized black carbon (BC) concentration under different velocities. The blue triangle and the red rectangle represent the BC normalized concentration under the westerly air masses and the easterly air masses, respectively.

In addition, the velocity of air masses from different directions also affects the BC concentration. By calculating the BC concentration at different velocities, we find that the influence of velocity on BC concentration under the easterly and westerly air masses is significantly different. As shown in Figure 5, the BC concentration under the easterly air masses increases with an increase of the velocity, and the BC concentration under the westerly air masses decreases with an increase of the velocity. The relationship between air masses velocity and BC concentration is as follows:

$$\varepsilon_e = 0.94 + 0.014v_e \qquad 0 < v_e < 7 \tag{10}$$

$$\varepsilon_w = 1.26 - 0.027v_w \qquad 0 < v_w < 18 \tag{11}$$

Table 2
Observational and Estimated BC Concentration of WLG in Four Seasons

Season	Observational concentration (ng/m³)	Estimated concentration (ng/m³) (1) $\tau_i = 0.58$[a]	(2) $BCe_i = 512$[b] $BCw_i = 444$	(3) $v_{ei} = 3.48$[c] $v_{wi} = 4.66$
Spring	486	529	455	519
Summer	484	484	484	484
Autumn	405	432	474	427
Winter	465	614	4,467	518

Note. BC, black carbon; WLG, Waliguan.
[a]Frequency of easterly air masses was constant as that in summer. [b]BC concentration under the easterly and westerly air masses was constants as that in summer. [c]Velocities of the easterly and westerly air masses were constants as those in summer.

where ε_e and ε_w represent the normalized BC concentrations (observed value/mean value) under the easterly and westerly air masses, v_e and v_w represent the velocity of easterly and westerly air masses (unit: m/s). Within the defined range of velocity, the proportions of easterly and westerly air mass trajectories are 99.4% and 96.3%, respectively. The correlation between ε and observed BC concentration under the easterly and westerly air masses is 0.78 and 0.98 with the significance level $p < 0.05$.

Therefore, considering the influence of air masses velocity on BC, Equation 9 can be expressed as follows:

$$BC_i = BCe_i \times \tau_i \times \frac{\varepsilon_{ei}'}{\varepsilon_{ei}} + BCw_i \times (1 - \tau_i) \times \frac{\varepsilon_{wi}'}{\varepsilon_{wi}} \quad (12)$$

where ε_{ei} and ε_{wi} represent the average normalized BC concentrations in month i under the easterly and westerly air masses, ε_{ei}' and ε_{wi}' represent the average normalized BC concentrations in month i under the easterly and westerly air masses when the velocity changes. If the air masses velocity is consistent with the observed value, $\varepsilon_{ei} = \varepsilon_{ei}'$, $\varepsilon_{wi} = \varepsilon_{wi}'$.

Hence, Equation 12 can be used to estimate BC concentration. Moreover, by comparing the seasonal BC variation under three sensitivity tests with the observations, we try to determine the dominant cause for the distinct BC seasonal variation at WLG. The three sensitivity tests were designed as follows:

Test 1: The monthly frequency of easterly air masses was kept constant using the summer value ($\tau_i = 0.58$, the highest value in the four seasons); the monthly BC concentration and velocity of the easterly and westerly air masses were consistent with the observations.

Test 2: The monthly frequency and velocity of the easterly and westerly air masses were consistent with the observation; the monthly BC concentrations under the easterly and westerly air masses were kept constant using the summer values ($BCe_i = 512$, $BCw_i = 444$, ng/m³).

Test 3: The monthly frequency and BC concentration of the easterly and westerly air masses were consistent with the observation; the monthly velocities of the easterly and westerly air masses were kept constant using the summer values ($v_{ei} = 3.48$, $v_{wi} = 4.66$, m/s).

Unlike the other stations, the BC concentration in summer at WLG was higher than that in winter (Ji et al., 2018; Yang et al., 2019). We used Equation 12 to calculate the BC concentration in the four seasons under the three tests, and the results are shown in Table 2. In Tests 1 and 3, the estimated BC concentration was higher than the observations in spring, autumn, and winter. In Test 2, the estimated BC concentration in winter and spring was lower than the observations, whereas the estimated autumn value was higher than the observation. According to Equation 12, the estimated BC depends on the velocity, frequency, and BC concentration of easterly/westerly air masses. In Tests 1 and 3, when the frequency and velocity of the easterly and westerly air masses adopt constants, respectively (summer average), instead of observed seasonal changes, the estimated BC concentration in winter is higher than that in summer. In Test 2, when the BC concentrations under the easterly and westerly air masses adopt constants (summer average) to replace the observed seasonal changes, the estimated BC concentration at WLG in summer remained higher than that in winter. This suggests that the seasonal variation in frequency and velocity of the easterly and westerly air masses causes the BC concentration at WLG to be higher in summer than that in winter.

3.2.2. Air Masses and Emission Influence on Annual BC Variation

The interannual variation of frequency and velocity of the easterly and westerly air masses is not as obvious as the seasonal variation (Table 3). This suggests that frequency and velocity of the easterly and westerly air masses contribute less to the BC interannual variation. To quantitatively assess the contribution of frequency and velocity of the easterly and westerly air masses to the interannual variation of BC concentration (based on Equation 12), the BC annual concentration can be expressed as follows:

Table 3
Annual Frequency and Velocity of the Easterly and Westerly Air Masses and Its Influence on BC Concentration at WLG (AC: Absolute Contribution; RC: Relative Contribution)

	Easterly air mass frequency			Moving velocity of air mass			
Year	τ_{yr}	AC (ng/m^3)	RC (%)	v_{eyr} (m/s)	v_{wyr} (m/s)	AC (ng/m^3)	RC (%)
2009	0.40	1.82	0.8	3.69	7.34	−4.2	−2.0
2010	0.34	−11.9	11.7	3.56	7.90	−4.4	4.4
2011	0.37	2.62	2.8	3.16	5.87	15.9	17.2
2012	0.33	−1.7	3.9	3.05	6.28	−3.8	8.8
2013	0.32	−0.9	0.5	3.51	5.33	5.9	−3.3
2014	0.38	4.9	6.5	3.32	5.38	−0.6	0.8
2015	0.33	−4.5	−34.6	3.78	7.15	−7.3	−55.4
2016	0.34	1.3	2.3	3.31	7.45	−2.6	−4.4
2017	0.28	−0.8	−10.0	2.57	7.15	0.89	10.9

Note. BC, black carbon; WLG, Waliguan.

$$\mathrm{BC}_{yr} = \mathrm{BC}e_{yr} \times \tau_{yr} \times \frac{\varepsilon_{eyr}'}{\varepsilon_{eyr}} + \mathrm{BC}w_{yr} \times \left(1 - \tau_{yr}\right) \times \frac{\varepsilon_{wyr}'}{\varepsilon_{wyr}} \quad (13)$$

where *yr* is the year, BC_{yr} is the average BC concentration in year yr, τ_{yr} is the easterly air mass frequency in year *yr*, BCe_{yr} and BCw_{yr} represent the average BC concentration under the easterly and westerly air masses in year *yr*, ε_{eyr} and ε_{wyr} represent the average normalized BC concentrations in year yr under the easterly and westerly air masses, ε_{eyr}' and ε_{wyr}' represent the average normalized BC concentrations in year yr under the easterly and westerly air masses when the velocity changes. If the air masses velocity is consistent with the observed value, $\varepsilon_{eyr} = \varepsilon_{eyr}'$, $\varepsilon_{wyr} = \varepsilon_{wyr}'$.

When the value of previous year is used as the easterly air mass frequency at WLG, the estimated BC concentration can be expressed as follows:

$$\mathrm{BC}_{yr}' = BCe_{yr} \times \tau_{yr-1} + \mathrm{BC}w_{yr} \times \left(1 - \tau_{yr-1}\right) \quad (14)$$

where BC_{yr}' is the estimated annual average BC concentration under hypothetical conditions and $\tau_{yr\text{-}1}$ is the easterly air masses frequency of previous year.

When the values of the previous year are used as the velocity of the easterly and westerly air masses at WLG, the estimated BC concentration can be expressed as follows:

$$\mathrm{BC}_{yr}' = \mathrm{BC}e_{yr} \times \tau_{yr} \times \frac{\varepsilon_{eyr-1}}{\varepsilon_{eyr}} + \mathrm{BC}w_{yr} \times \left(1 - \tau_{yr}\right) \times \frac{\varepsilon_{wyr-1}}{\varepsilon_{wyr}} \quad (15)$$

where $\varepsilon_{eyr\text{-}1}$ and $\varepsilon_{wyr\text{-}1}$ represent normalized BC concentrations under the easterly and westerly air masses calculated based on the velocity of the previous year.

Thus, the contribution of the frequency or velocity of the easterly and westerly air masses to the interannual variation of BC concentration at WLG can be expressed as follows:

$$C_{yr} = \frac{\mathrm{BC}_{yr} - \mathrm{BC}_{yr}'}{\mathrm{BC}_{yr} - \mathrm{BC}_{yr-1}} \quad (16)$$

where C_{yr} is the contribution of frequency or velocity of the easterly and westerly air masses in year yr, $\mathrm{BC}_{yr\text{-}1}$ is the average BC concentration of the previous year, denominator is the observed BC concentration difference for continuous 2 years, and numerator is the estimated BC concentration variation caused by change of air masses. If $C_{yr} < 0$, it means that the increase/decrease of BC concentration estimated by frequency or velocity of the easterly and westerly air masses is inconsistent with the observed interannual variation. For example, in 2015, the estimated BC concentration at WLG was lower than that of the previous year, but the observed BC concentration at WLG increased. Therefore, we deduce that the frequency or velocity of the easterly and westerly air masses has a negative contribution to the BC interannual variation in 2015.

As shown in Table 3, the frequency and velocity of the easterly and westerly air masses do not contribute substantially to the interannual variation of WLG BC. The influence of the easterly air mass frequency on the interannual BC variation ranged from 0.9 to 11.9 ng/m^3. In 2015, the relative contribution of the easterly air mass frequency reached 34.6% but the influence concentration was only 4.5 ng/m^3. The influence of velocity of air masses on the interannual BC variation ranged from 0.6 to 15.9 ng/m^3 and its relative contribution is also at a low level.

The decreasing BC trend at WLG may also be affected by the reduction of surrounding emissions. According to the China Statistical Yearbook (2018), the proportion of coal in China's total energy consumption has continually decreased over the past 10 years (71.5% in 2008 vs. 60.4% in 2017), and the proportion of natural gas, primary power, and other energy has increased rapidly (10.1% in 2006 vs. 20.8% in 2017). The

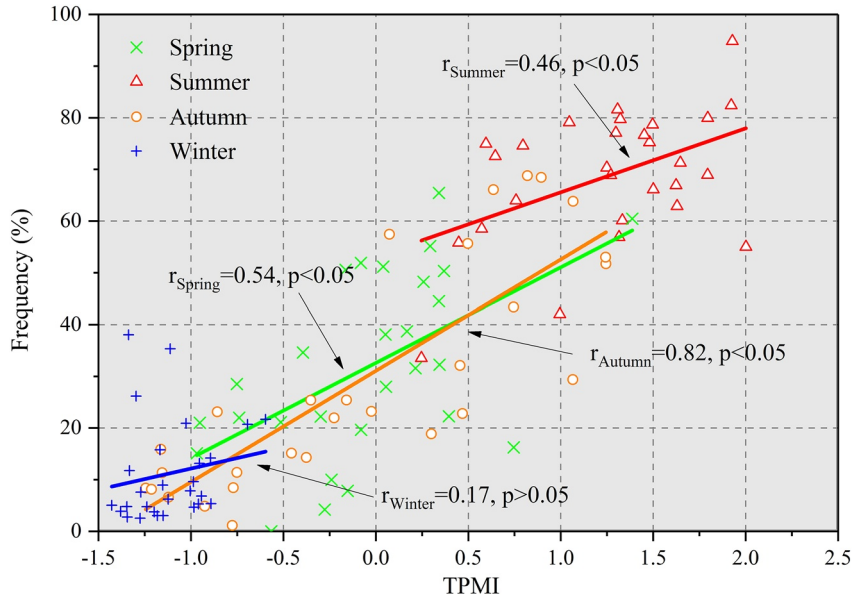

Figure 6. The relationship between the monthly TPMI and the easterly air mass frequency at Waliguan (WLG) in different seasons.

proportion of thermal power in the installed power generation capacity also decreased from 76.05% (2008) to 62.24% (2017), and the proportion of clean energy, such as hydropower, nuclear power, and wind power, increased. The implementation of several air pollution mitigation measures (e.g., improvements in industrial emission standards (power plants and emission-intensive industrial sectors), upgrades to industrial boilers, strengthening vehicle emission standards ("China 5" standard applied nationally and eliminated 20 million old vehicles), phasing out of outdated industrial capacities, and the application of clean fuels in the residential sector) has collectively decreased the major pollutant emissions and significantly improved air quality in China in 2013–2017 (Y. Wang et al., 2019; Q. Zhang, Zheng, et al., 2019). We also observed a decreasing trend in the BC concentration at sites around WLG (Figure 2b). The resulting improvement of air quality reduced the pollutant transport to WLG, which decreased BC concentrations at this site.

3.2.3. Effect of the Tibetan Plateau Monsoon on BC Transport

The previous sections demonstrated the importance of the easterly air mass frequency in controlling the distinct seasonal BC variation at WLG as well as its certain influence on the interannual BC variation.

The unique topography and thermal conditions of the TP play an important role in the variation of atmospheric circulation in Asia. The TP serves as a powerful heat source in summer, heating the air directly in the middle of the troposphere (Flohn, 1957, 1960). The air over the TP ascends in summer, which drives the convergence of the surrounding surface air to the TP. Hence, the circulation over the plateau tends to be cyclonic during the summer, which subsequently forms the Tibetan Plateau monsoon (Ge et al., 2017; Tang et al., 1998; Wu et al., 2012). WLG is located northeast of the TP. The highest easterly air mass frequency at WLG (induced by the Asian summer monsoon) may be further enhanced by the influence of the Tibetan Plateau monsoon in the northeastern TP in summer (Zhu et al., 2016).

We calculated the dynamically normalized seasonality monsoon index over the region 27–38°N and 80–100°E to obtain a Tibetan Plateau monsoon index (TPMI), which reflects the convergence intensity of wind field over the TP. As shown in Figure 6, significant positive correlations were observed between TPMI and the easterly air mass frequency at WLG in spring, summer, and autumn, with correlation coefficients of 0.54, 0.46, and 0.82 ($P < 0.05$). We inferred that the Tibetan Plateau monsoon significantly influenced the interannual variation of the easterly air mass frequency at WLG. Furthermore, the change of the easterly air mass frequency would modulate the BC contributions from polluted eastern regions to WLG in summer. In addition, we found that the correlation coefficient between the whole monthly TPMI and easterly air mass

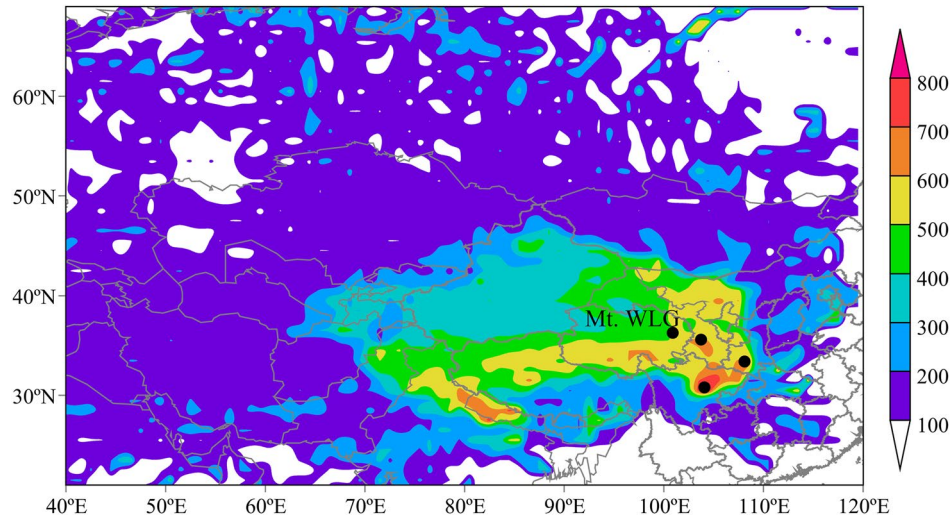

Figure 7. Concentration-weighted trajectory (96 hr) in 2008–2017 at Waliguan (WLG). The color bar on the right is black carbon mass concentration in ng/m^3. (The black dots to the east of WLG correspond to Lanzhou, Chengdu, and Xi'an).

frequency at WLG was 0.87 ($p < 0.05$). In summer (winter), the Tibetan Plateau monsoon is strong (weak) and the easterly air mass frequency at WLG is high (low).

3.3. Source Apportionment of WLG BC

3.3.1. Concentration-Weighted Trajectory

To further understand the contribution of different regions to the BC concentration at WLG, we used the CWT to identify high-potential source regions. Based on the CWT results (Figure 7), we identified Lanzhou, Chengdu, and Xi'an urban agglomerations east of WLG to be the high-potential BC source regions (>600 ng/m^3). These regions are located near WLG and are densely populated, highly industrialized and commercialized, and heavily polluted. Central Qinghai, northern Tibet (500–600 ng/m^3), and northern India (>600 ng/m^3) were also significant contributors. Northern India is one of the most polluted areas in South Asia due to its high population density and large anthropogenic emissions (Lal et al., 2012; Ram et al., 2012). In contrast, only a few industries occur in the TP, and hydropower is the main energy source. Moreover, the TP region is generally short of conventional energy (coal and petroleum) but rich in renewables (water conservancy, wind, and geothermal) (Ping et al., 2011). The TP has low BC emissions, and the high CWT value in this region is not consistent with its BC emissions scale. We can infer that central Qinghai and northern Tibet are the long-distance transport pathways from northern India to WLG.

3.3.2. Modeled Contribution of Different Regions to WLG BC

In this section, we quantified the average (2008–2014) regional contributions to seasonal BC at WLG by CAM5 with BC-tagging technique. The horizontal resolution of the simulation is 1.9° × 2.5° and 56 vertical levels from the ground to 4 hPa. The Modern-Era Retrospective analysis for Research and Applications (MERRA) data sets with a time resolution of 6 hr was used to nudge the meteorology fields (Rienecker et al., 2011). The emission inventory, BC-tagging method, and other model settings as well as model validation are detailed in Fang et al. (2020). The NME (normalized mean error, NME = $100\% \times \Sigma|(Mi-Oi)|/\Sigma Oi$, where i represents month, M represents the simulated value, and O represents the observed value) for BC at WLG was found to be 34%. The model also captures the seasonal characteristics of BC concentration observed at WLG in which summer is higher than in winter (Figure 8b). The monthly correlation coefficient is 0.5 with the significance level $p < 0.01$. Hence, the CESM model can reasonably reproduce the BC concentration level and temporal variation.

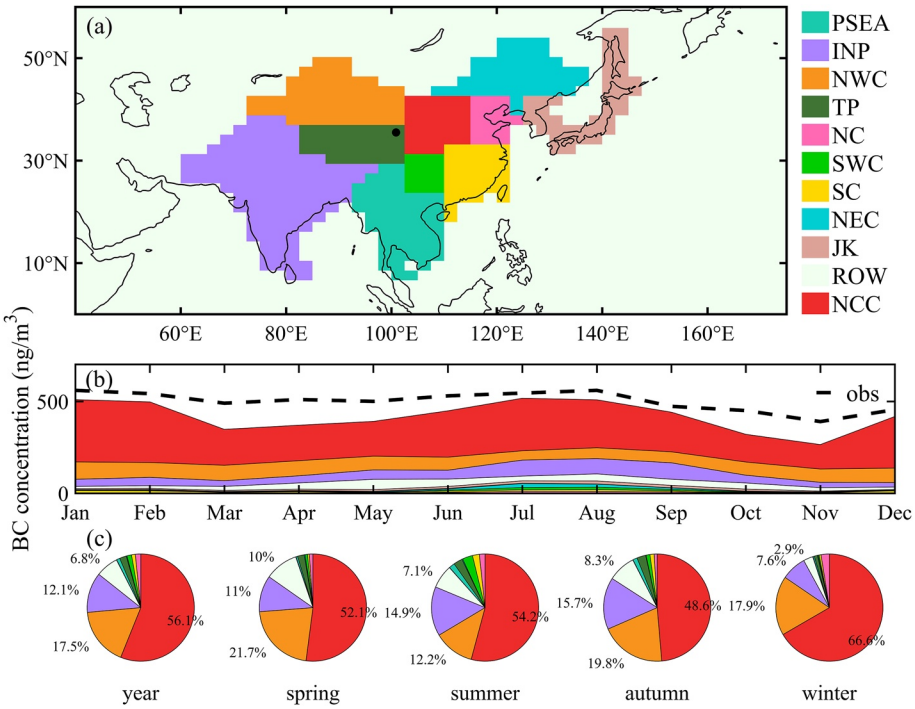

Figure 8. Tagged source regions in black carbon (BC)-tagging method, the black dot indicates Mt. Waliguan (WLG) (a), average absolute contribution (ng/m^3) of tagged regions to the BC concentration at WLG in 2008–2014, the black dashed line indicates the observed value (b), average relative contribution (%) of tagged source regions to BC concentration at WLG in 2008–2014 (c), relative contributions less than 2% are not shown.

As shown in Figure 8a, there are 11 source regions, namely, North Central China (NCC), Northwest China (NWC), Indian Peninsula (INP), Tibetan Plateau (TP), North China (NC), Southwest China (SWC), South China (SC), Peninsula Southeast Asia (PSEA), Northeast China (NEC), Japan and South Korea (JK), and rest of world (ROW).

The absolute contribution of the different tagged source regions to the WLG BC concentration showed seasonal variation (Figure 8b), and the contribution from the region east of WLG was significantly greater than that from the west. Under the influence of the Asian summer monsoon, the absolute contribution of INP, SWC, SC, and SEAP in summer was significantly higher than that in other seasons, while NWC showed the lowest contribution due to the weakest prevailing westerlies in summer. In Section 3.1, we can find that the westerly frequency at WLG decreases in summer, but due to the influence of the Indian monsoon, the southwest wind accounts for most of the westerly wind (the northwest wind is dominant in winter), which explains the high BC absolute contribution from INP in summer.

Figure 8c shows the relative BC contributions from regional sources to WLG. We identified three main BC source regions with respect to WLG, including NCC (56.1%), NWC (17.5%), and INP (12.1%), which is similar to the results of previous studies (Han et al., 2020; Yang et al., 2018; R. Zhang et al., 2015). Among them, NCC and INP are high BC emission regions. NWC is adjacent to WLG, and prevailing westerly winds are conducive to BC transport in this region. The TP is sparsely populated, with underdeveloped industries and low BC emissions, contributing only 2.1% to the total BC at WLG. The NCC, INP, and NWC significantly contributed to the BC concentration at WLG, which is consistent with the high-potential source regions identified from the CWT. The TP showed little BC contribution, and central Qinghai and northern Tibet are located within the BC transport pathway from northern India to WLG.

4. Conclusions

In this study, we used the CBNET data set to analyze the characteristics and influencing factors on diurnal, seasonal, and long-term BC trends at WLG from 2008 to 2017. The main potential source regions and quantitative contributions of BC were also identified by CWT and CAM5.

The average BC concentration at WLG was 449 ± 366 ng/m^3. The seasonal average BC concentration occurred in the order of spring (487 ng/m^3) ≈summer (484 ng/m^3) > winter (465 ng/m^3) > autumn (406 ng/m^3) and the diurnal BC peak value occurred at noon. The BC concentration showed a decreasing trend of −2%yr^{-1} from 2008 to 2017, which was mainly due to the implementation of emission reduction measures in China.

The BC concentration at WLG was higher under easterly air masses than under westerly air masses. The variations in frequency and velocity of the easterly and westerly air masses are the main factors for the distinct seasonal BC variation (summer > winter) at WLG. The Tibetan Plateau monsoon has a significant impact on the interannual variation of easterly air mass frequency at WLG and further modulates the BC contributions from polluted eastern regions to WLG.

According to the CWT results, the high-potential source regions of BC to WLG were mainly Lanzhou, Chengdu, and Xi'an urban agglomerations as well as northern India. Based on the CAM5 quantitative analysis, NCC, NWC, and INP showed the highest BC contribution (annual average) to WLG, accounting for 56.1%, 17.5%, and 12.1% of the total BC, respectively.

Data Availability Statement

The HYSPLIT model can be acquired from http://www.arl.noaa.gov/HYSPLIT_info.php. The Peking University BC inventory is available from http://inventory.pku.edu.cn/home.html. The CESM code is available from https://svn-ccsm-release.cgd.ucar.edu/model_versions/. The username is guestuser and the password is friendly. The NCEP/NCAR reanalysis is available from https://psl.noaa.gov/data/gridded/data.ncep.reanalysis.html. The data presented in this article can be acquired from https://zenodo.org/record/5520533. The MeteoInfo software can be acquired from http://meteothink.org/.

Acknowledgments
This work is supported by grants from the National Key Research and Development Program of China (2016YFA0602003) and National Natural Science Foundation of China (42021004, 41605091, 41805120). We greatly thank all the CBNET investigators for the great efforts and support over the years in maintaining the network and collecting data. The CWT analysis and spatial distribution of annual mean BC concentration were conducted by MeteoInfo_2.2.1_2 and ArcGIS 10.3, respectively. The Tibetan Plateau monsoon index and trends of BC concentration were conducted based on Matlab 2016b.

References

Babu, S. S., Satheesh, S. K., & Moorthy, K. K. (2002). Aerosol radiative forcing due to enhanced black carbon at an urban site in India. *Geophysical Research Letters*, *29*(18), 27–1274. https://doi.org/10.1029/2002GL015826

Bond, T. C., Doherty, S. J., Fahey, D. W., Forster, P. M., Berntsen, T., Deangelo, B., et al. (2013). Bounding the role of black carbon in the climate system: A scientific assessment. *Journal of Geophysical Research: Atmospheres*, *118*(11), 5380–5552. https://doi.org/10.1002/jgrd.50171

Bycenkienė, S., Ulevicius, V., & Kecorius, S. (2011). Characteristics of black carbon aerosol mass concentration over the East Baltic region from two-year measurements. *Journal of Environmental Monitoring*, *13*(4), 1027–1038. https://doi.org/10.1039/c0em00480d

Cao, J., Xu, B., He, J., Liu, X., Han, Y., Wang, G., & Zhu, C. (2009). Concentrations, seasonal variations, and transport of carbonaceous aerosols at a remote Mountainous region in western China. *Atmospheric Environment*, *43*(29), 4444–4452. https://doi.org/10.1016/j.atmosenv.2009.06.023

Cape, J. N., Coyle, M., & Dumitrean, P. (2012). The atmospheric lifetime of black carbon. *Atmospheric Environment*, *59*, 256–263. https://doi.org/10.1016/j.atmosenv.2012.05.030

Cerqueira, M., Pio, C., Legrand, M., Puxbaum, H., Kaspergiebl, A., Afonso, J., et al. (2010). Particulate carbon in precipitation at European background sites. *Journal of Aerosol Science*, *41*(1), 51–61. https://doi.org/10.1016/j.jaerosci.2009.08.002

Chen, X., Kang, S., Cong, Z., Yang, J., & Ma, Y. (2018). Concentration, temporal variation, and sources of black carbon in the Mt. Everest region retrieved by real time observation and simulation. *Atmospheric Chemistry and Physics*, *18*(17), 12859–12875. https://doi.org/10.5194/acp-18-12859-2018

CSY. (2018). *China statistical Yearbook*. China Statistical Publishing House.

Deng, X., Tie, X., Wu, D., Zhou, X., Bi, X., Tan, H., et al. (2008). Long-term trend of visibility and its characterizations in the Pearl River Delta (PRD) region, China. *Atmospheric Environment*, *42*(7), 1424–1435. https://doi.org/10.1016/j.atmosenv.2007.11.025

Fang, C., Zhu, B., Pan, C., Yun, X., Ding, D., & Tao, S. (2020). Regional and sectoral sources for black carbon over South China in spring and their sensitivity to East Asian summer monsoon onset. *Journal of Geophysical Research: Atmospheres*, *125*(20), e2020JD033219. https://doi.org/10.1029/2020JD033219

Flohn, H. (1957). Large-scale aspects of the "Summer Monsoon" in South and East Asia. *Journal of the Meteorological Society of Japan*, *35A*, 180–186. https://doi.org/10.2151/jmsj1923.35A.0_180

Flohn, H. (1960). *Recent investigations on the mechanism of the" summer monsoon" of southern and eastern Asia*. Monsoons of the World.

Fu, X. W., Feng, X., Liang, P., Zhang, H., Ji, J., & Liu, P. (2012). Temporal trend and sources of speciated atmospheric mercury at Waliguan GAW station, Northwestern China. *Atmospheric Chemistry and Physics*, *12*, 4. https://doi.org/10.5194/acp-12-1951-2012

Ge, F., Sielmann, F., Zhu, X., Fraedrich, K., Zhi, X., Peng, T., & Wang, L. (2017). The link between Tibetan Plateau monsoon and Indian summer precipitation: A linear diagnostic perspective. *Climate Dynamics*, *49*(11), 4201–4215. https://doi.org/10.1007/s00382-017-3585-1

Han, H., Wu, Y., Liu, J., Zhao, T., Zhuang, B., Wang, H., et al. (2020). Impacts of atmospheric transport and biomass burning on the inter-annual variation in black carbon aerosols over the Tibetan Plateau. *Atmospheric Chemistry and Physics*, *20*(21), 13591–13610. https://doi.org/10.5194/acp-20-13591-2020

Hansen, J., & Nazarenko, L. (2004). Soot climate forcing via snow and ice albedos. *Proceedings of the National Academy of Sciences of the United States of America*, *101*(2), 423–428. https://doi.org/10.1073/pnas.2237157100

Janssen, N. A., Hoek, G., Simic-Lawson, M., Fischer, P., Van Bree, L., Ten Brink, H., et al. (2011). Black carbon as an ad-ditional indicator of the adverse health effects of airborne particles compared with PM10 and PM2.5. *Environmental Health Perspectives*, *119*(12), 1691–1699. https://doi.org/10.1289/ehp.1003369

Ji, D., Li, L., Pang, B., Xue, P., Wang, L., Wu, Y., et al. (2017). Characterization of black carbon in an urban-rural fringe area of Beijing. *Environmental Pollution*, *223*, 524–534. https://doi.org/10.1016/j.envpol.2017.01.055

Ji, D., Yan, Y., Wang, Z., He, J., Liu, B., Sun, Y., et al. (2018). Two-year continuous measurements of carbonaceous aerosols in urban Beijing, China: Temporal variations, characteristics and source analyses. *Chemosphere*, *200*, 191–200. https://doi.org/10.1016/j.chemosphere.2018.02.067

Joshi, R., Liu, D., Nemitz, E., Langford, B., Mullinger, N., Squires, F., et al. (2021). Direct measurements of black carbon fluxes in central Beijing using the eddy covariance method. *Atmospheric Chemistry and Physics*, *21*(1), 147–162. https://doi.org/10.5194/ACP-21-147-2021

Kang, H., Zhu, B., Der A, R. V., Zhu, C., De Leeuw, G., Hou, X., & Gao, J. (2019). Natural and anthropogenic contributions to long-term variations of SO2, NO2, CO, and AOD over East China. *Atmospheric Research*, *215*, 284–293. https://doi.org/10.1016/J.ATMOSRES.2018.09.012

Kendall, M. G. (1975). *Rank correlation methods* (4th ed.). Charles Griffin.

Koelmans, A. A., Jonker, M. T., Cornelissen, G., Bucheli, T. D., Van Noort, P. C., & Gustafsson, O. (2006). Black carbon: The reverse of its dark side. *Chemosphere*, *63*(3), 365–377. https://doi.org/10.1016/j.chemosphere.2005.08.034

Lal, D. M., Ghude, S. D., Patil, S. D., Kulkarni, S. H., Jena, C., Tiwari, S., & Srivastava, M. K. (2012). Tropospheric ozone and aerosol long-term trends over the Indo-Gangetic Plain (IGP), India. *Atmospheric Research*, *116*, 82–92. https://doi.org/10.1016/j.atmosres.2012.02.014

Li, B., Gasser, T., Ciais, P., Piao, S., Tao, S., Balkanski, Y., et al. (2016). The contribution of China's emissions to global climate forcing. *Nature*, *531*(7594), 357–361. https://doi.org/10.1038/nature17165

Li, J. P., & Zeng, Q. C. (2002). A unified monsoon index. *Geophysical Research Letters*, *29*(8), 1151–1154. https://doi.org/10.1029/2001GL013874

Li, J. P., & Zeng, Q. C. (2003). A new monsoon index and the geographical distribution of the global monsoons. *Advances in Atmospheric Sciences*, *20*(2), 299–302. https://doi.org/10.1007/s00376-003-0016-5

Li, R., Wang, Z., Cui, L., Fu, H., Zhang, L., Kong, L., et al. (2019). Air pollution characteristics in China during 2015-2016: Spatiotemporal variations and key meteorological factors. *The Science of the Total Environment*, *648*, 902–915. https://doi.org/10.1016/j.scitotenv.2018.08.181

Lin, W., Dai, J., Liu, R., Zhai, Y., Yue, D., & Hu, Q. (2019). Integrated assessment of health risk and climate effects of black carbon in the Pearl River Delta region, China. *Environmental Research*, *176*, 108522. https://doi.org/10.1016/j.envres.2019.06.003

Lu, Y., Zhu, B., Huang, Y., Shi, S., Wang, H., An, J., & Yu, X. (2019). Vertical distributions of black carbon aerosols over rural areas of the Yangtze River Delta in winter. *The Science of the Total Environment*, *661*, 1–9. https://doi.org/10.1016/j.scitotenv.2019.01.170

Menon, S., Hansen, J., Nazarenko, L., & Luo, Y. (2002). Climate effects of black carbon aerosols in China and India. *Science*, *297*(5590), 2250–2253. https://doi.org/10.1126/science.1075159

Pan, X., Kanaya, Y., Wang, Z., Liu, Y., Pochanart, P., Akimoto, H., et al. (2011). Correlation of black carbon aerosol and carbon monoxide in the high-altitude environment of Mt. Huang in Eastern China. *Atmospheric Chemistry and Physics*, *11*(18), 9735–9747. https://doi.org/10.5194/acp-11-9735-2011

Pani, S. K., Wang, S. H., Lin, N. H., Chantara, S., Lee, C. T., & Thepnuan, D. (2020). Black carbon over an urban atmosphere in northern peninsular Southeast Asia: Characteristics, source apportionment, and associated health risks. *Environmental Pollution*, *259*, 113871. https://doi.org/10.1016/j.envpol.2019.113871

Peng, X., Liu, M., Zhang, Y., Meng, Z., Achal, V., Zhou, T., et al. (2019). The characteristics and local-regional contributions of atmospheric black carbon over urban and suburban locations in Shanghai, China. *Environmental Pollution*, *255*, 113188. https://doi.org/10.1016/j.envpol.2019.113188

Ping, X., Jiang, Z., & Li, C. (2011). Status and future perspectives of energy consumption and its ecological impacts in the Qinghai–Tibet region. *Renewable and Sustainable Energy Reviews*, *15*(1), 514–523. https://doi.org/10.1016/j.rser.2010.07.037

Rajesh, T. A., & Ramachandran, S. (2017). Characteristics and source apportionment of black carbon aerosols over an urban site. *Environmental Science and Pollution Research*, *24*(9), 8411–8424. https://doi.org/10.1007/s11356-017-8453-3

Ram, K., Sarin, M. M., & Tripathi, S. N. (2012). Temporal trends in atmospheric PM2. 5, PM10, elemental carbon, organic carbon, water-soluble organic carbon, and optical properties: Impact of biomass burning emissions in the Indo-Gangetic Plain. *Environmental Science & Technology*, *46*(2), 686–695. https://doi.org/10.1021/es202857w

Rienecker, M. M., Suarez, M. J., Gelaro, R., Todling, R., Bacmeister, J., Liu, E., et al. (2011). MERRA: NASA's modern-era retrospective analysis for research and applications. *Journal of Climate*, *24*(14), 3624–3648. https://doi.org/10.1175/JCLI-D-11-00015.1

Rodhe, H., Persson, C., & Akesson, O. (1972). An investigation into regional transport of soot and sulfate aerosols. *Atmospheric Environment*, *6*(9), 675–693. https://doi.org/10.1016/0004-6981(72)90025-X

Sarkar, C., Roy, A., Chatterjee, A., Ghosh, S. K., & Raha, S. (2019). Factors controlling the long-term (2009-2015) trend of PM2.5 and black carbon aerosols at eastern Himalaya, India. *The Science of the Total Environment*, *656*, 280–296. https://doi.org/10.1016/j.scitotenv.2018.11.367

Seibert, P., Kromp-Kolb, H., Baltensperger, U., Jost, D. T., Schwikowski, M., Kasper, A., & Puxbaum, H. (1994). Trajectory analysis of aerosol measurements at high alpine sites. *Transport and Transformation of Pollutants in the Troposphere*, *15*(9), 689–693.

Tang, M., Cheng, G., & Lin, Z. (1998). *Contemporary climatic variations over Qinghai-Xizang (Tibetan) Plateau and their influences on environments* (p. 339). Qing Zang Gaoyuan yan jiu cong shu.

Trompetter, W. J., Grange, S. K., Davy, P. K., & Ancelet, T. (2013). Vertical and temporal variations of black carbon in New Zealand urban areas during winter. *Atmospheric Environment*, *75*, 179–187. https://doi.org/10.1016/j.atmosenv.2013.04.036

Wang, M., Xu, B., Wang, N., Cao, J., Tie, X., Wang, H., et al. (2016). Two distinct patterns of seasonal variation of airborne black carbon over Tibetan Plateau. *The Science of the Total Environment*, *573*, 1041–1052. https://doi.org/10.1016/j.scitotenv.2016.08.184

Wang, Q., Schwarz, J. P., Cao, J., Gao, R., Fahey, D. W., Hu, T., et al. (2014). Black carbon aerosol characterization in a remote area of Qinghai–Tibetan Plateau, western China. *The Science of the Total Environment*, *479*, 151–158. https://doi.org/10.1016/j.scitotenv.2014.01.098

Wang, X., Xu, B., & Ming, J. (2014). An overview of the studies on black carbon and mineral dust deposition in snow and ice cores in East Asia. *Journal of Meteorological Research*, *28*(3), 354–370. https://doi.org/10.1007/s13351-014-4005-7

Wang, Y., Li, W., Gao, W., Liu, Z., Tian, S., Shen, R., et al. (2019). Trends in particulate matter and its chemical compositions in China from 2013–2017. *Science China Earth Sciences*, *62*(12), 1857–1871. https://doi.org/10.1007/s11430-018-9373-1

Wu, G., Liu, Y., He, B., Bao, Q., Duan, A., & Jin, F. (2012). Thermal controls on the Asian summer monsoon. *Scientific Reports*, *2*(1), 404–404. https://doi.org/10.1038/srep00404

Yang, J., Kang, S., Ji, Z., & Chen, D. (2018). Modeling the origin of anthropogenic black carbon and its climatic effect over the Tibetan Plateau and surrounding regions. *Journal of Geophysical Research: Atmospheres*, *123*(2), 671–692. https://doi.org/10.1002/2017JD027282

Yang, Y., Xu, X., Zhang, Y., Zheng, S., Wang, L., Liu, D., et al. (2019). Seasonal size distribution and mixing state of black carbon aerosols in a polluted urban environment of the Yangtze River Delta region, China. *The Science of the Total Environment*, *654*, 300–310. https://doi.org/10.1016/j.scitotenv.2018.11.087

Zhang, Q., Yu, R., Jin, Y., Zhang, Z., Liu, X., Xue, H., et al. (2019). Temporal and spatial variation trends in water quality based on the WPI index in the shallow lake of an arid area: A case study of Lake Ulansuhai, China. *Water*, *11*(7), 1410. https://doi.org/10.3390/w11071410

Zhang, Q., Zheng, Y., Tong, D., Shao, M., Wang, S., Zhang, Y., et al. (2019). Drivers of improved PM2.5 air quality in China from 2013 to 2017. *Proceedings of the National Academy of Sciences of the United States of America*, *116*(49), 24463–24469. https://doi.org/10.1073/pnas.1907956116

Zhang, R., Wang, H., Qian, Y., Rasch, P. J., Easter, R. C., Ma, P., et al. (2015). Quantifying sources, transport, deposition and radiative forcing of black carbon over the Himalayas and Tibetan Plateau. *Atmospheric Chemistry and Physics*, *15*(11), 6205–6223. https://doi.org/10.5194/acp-15-6205-2015

Zhang, X. Y., Wang, Y. Q., Zhang, X. C., Guo, W., & Gong, S. L. (2008). Carbonaceous aerosol composition over various regions of china during 2006. *Journal of Geophysical Research*, *113*(D14). https://doi.org/10.1029/2007JD009525

Zhang, Y., Li, Y., Guo, J., Wang, Y., Chen, D., & Chen, H. (2019). The climatology and trend of black carbon in China from 12-year ground observations. *Climate Dynamics*, *53*, 5881–5892. https://doi.org/10.1007/s00382-019-04903-0

Zhou, J. M., Zhang, R. J., Cao, J. J., Chow, J. C., & Watson, J. G. (2012). Carbonaceous and ionic components of atmospheric fine particles in Beijing and their impact on atmospheric visibility. *Aerosol & Air Quality Research*, *12*(4), 492–502. https://doi.org/10.4209/aaqr.2011.11.0218

Zhu, B., Hou, X., & Kang, H. (2016). Analysis of the seasonal ozone budget and the impact of the summer monsoon on the northeastern Qinghai-Tibetan Plateau. *Journal of Geophysical Research: Atmospheres*, *121*(4), 2029–2042. https://doi.org/10.1002/2015JD023857

Zhuang, B. L., Wang, T. J., Liu, J., Li, S., Xie, M., Yang, X. Q., et al. (2014). Continuous measurement of black carbon aerosol in urban Nanjing of Yangtze River Delta, China. *Atmospheric Environment*, *89*, 415–424. https://doi.org/10.1016/j.atmosenv.2014.02.052